Hydrology Research

Hydrology Research Vol 53 No 11, 1393 doi: 10.2166/nh.2022.062

Wet-environment Evapotranspiration and Precipitation Standardized Index (WEPSI) for drought assessment and monitoring

Ali Khoshnazar [a], Gerald A. Corzo Perez [a,b], Vitali Diaz [a,b,*], Milad Aminzadeh [c] and Roberto Adolfo Cerón Pineda [d]

[a] IHE Delft Institute for Water Education, Delft, The Netherlands
[b] Delft University of Technology, Delft, The Netherlands
[c] Institute of Geo-Hydroinformatics, Hamburg University of Technology, Hamburg, Germany
[d] Ministry of the Environment and Natural Resources (MARN), San Salvador, El Salvador
*Corresponding author. E-mail: v.diazmercado@tudelft.nl; vitalidime@gmail.com

AK, 0000-0002-7122-6432; GACP, 0000-0002-2773-7817; VD, 0000-0002-5502-4099; MA, 0000-0002-0074-3600

ABSTRACT

Drought assessment and monitoring are essential for its proper management. Drought indices play a fundamental role in this. This research introduces the Wet-environment Evapotranspiration and Precipitation Standardized Index (WEPSI) for drought assessment and monitoring. WEPSI incorporates water supply and demand into the drought index calculation. WEPSI considers precipitation (P) for water supply and wet-environment evapotranspiration (ET_w) for water demand. We use an asymmetric complementary relationship to calculate ET_w with actual (ET_a) and potential evapotranspiration (ET_p). WEPSI is tested in the transboundary Lempa River basin in the Central American dry corridor. ET_w is estimated based on evapotranspiration data calculated using the Water Evaluation And Planning (WEAP) system hydrological model. To investigate the performance of WEPSI, we compare it with two well-known meteorological indices (Standardized Precipitation Index and Standardized Precipitation Evapotranspiration Index), together with a hydrological index (Standardized Runoff Index), in terms of statistical metrics and mutual information (MI). We compare WEPSI-derived droughts and historical information, including crop production, cereal yield, and the Oceanic Nino Index (ONI). Results show WEPSI has the highest correlation and MI, and the lowest deviation. It is consistent with the records of the crop production index, cereal yield, and the ONI. Findings show that WEPSI can be used for agricultural drought assessments.

Key words: drought index, Lempa River basin, mutual information, WEAP, WEPSI, wet-environment evapotranspiration

HIGHLIGHTS

- WEPSI for drought assessment and monitoring is introduced.
- A step-by-step methodology for calculating WEPSI, including the computation of wet-environment evapotranspiration is presented.
- Spatiotemporal analysis of drought with hydrological modeling data and WEPSI is illustrated.
- WEPSI is suitable for running on remote sensing data.
- Results indicate WEPSI for agricultural and hydrological drought applications.

GRAPHICAL ABSTRACT

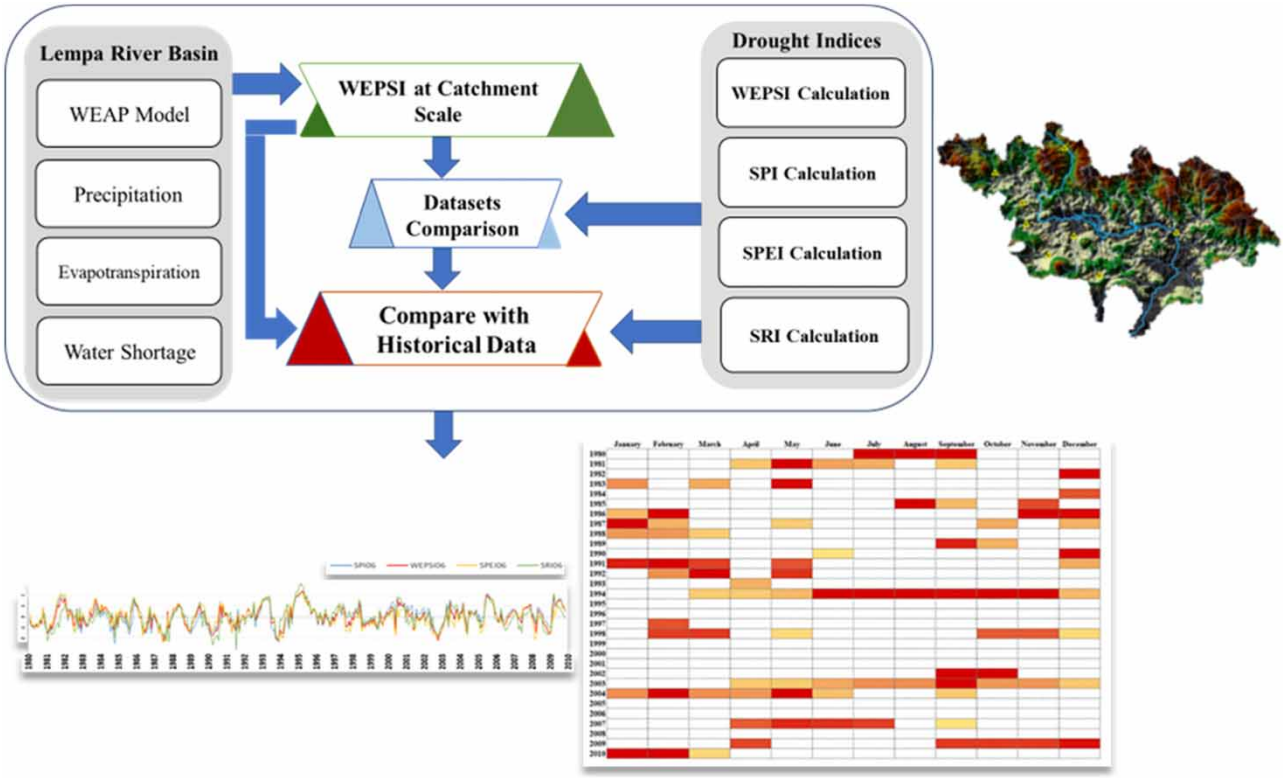

1. INTRODUCTION

Drought affects around 40% of the global land area and is a major threat to global agriculture (Wang *et al.* 2011; Wen *et al.* 2021). It can trigger or intensify wildfire, water scarcity, crop damage, food price increase, migration, and adverse health impacts (Mukherjee *et al.* 2018; Tabari *et al.* 2021). Drought monitoring is crucial to prepare for drought and mitigate its negative effects (Fanok *et al.* 2022). In this regard, drought indices are useful measures for scientists and decision-makers to monitor, assess, and manage drought.

Although there exists no unique standard definition for drought, it is described as the deficit in precipitation (P) compared with an average within a period (Yihdego *et al.* 2019; Wang *et al.* 2020). The combination of anomalies in P and temperature, known as meteorological drought, leads to soil moisture deficit, referred to as agricultural drought, and a lack of water in lakes and streams, defined as hydrological drought (Wilhite & Glantz 1985; Mukherjee *et al.* 2018). Agricultural and hydrological droughts are usually the subsequent phases of meteorological drought (Peters *et al.* 2003).

A drought index aims to quantify drought severity and help in the identification and characterization of drought development by assimilating a hydrometeorological dataset into numerical values that indicate the magnitude of water anomalies. Selecting a proper drought index for drought assessment and monitoring is not always trivial and involves different challenges. The following considerations should be made when selecting the drought index. (1) The drought index must follow the standardization of the hydrometeorological variable used. Otherwise, in contiguous regions, the same drought index can show different drought conditions, making it difficult to calculate drought onset and spatial extent. (2) It is preferable that the methodology for the calculation is clear and that the fewest possible inputs are used. Some drought indices are not usable everywhere. Some others require many inputs or have complex structures that make their implementation difficult. (3) It is desirable if the drought index can identify different types of droughts. Some drought indices can detect various types of droughts, making them have a broader range of applications (Yihdego *et al.* 2019).

Much academic effort has been devoted to introducing appropriate drought indices (Abdelkader & Yerdelen 2021). As an early attempt, Palmer (1965) proposed a regional index to determine meteorological and agricultural droughts, known as the Palmer Drought Severity Index (PDSI). The PDSI uses temperature, soil moisture, and P. The structure of the PDSI does not

allow for comparison across different regions. Time scale limitation and data complexity are also highlighted deficiencies of the PDSI. Based on these drawbacks, 3 years later, Palmer introduced his Crop Moisture Index (CMI) for agricultural drought (Palmer 1968). The self-calibrated Palmer Drought Severity Index (scPDSI), proposed by Wells *et al.* (2004), is another index based on the PDSI but allows comparison of different regions.

One of the most outstanding advances in developing drought indices was made by McKee *et al.* (1993). They proposed one of the most well-known drought indices, the Standardized Precipitation Index (SPI). The SPI is popular because of its simple structure. It can be calculated with the presence of missing data. The SPI has the flexibility of calculation in short or long time steps (aggregation periods) (Sutanto & Van Lanen 2021), which is especially advantageous in monitoring different types of droughts (Vicente-Serrano *et al.* 2010; Yihdego *et al.* 2019). Nevertheless, the SPI overlooks the role of other important variables, such as evapotranspiration (ET) (Vicente-Serrano *et al.* 2010; Mukherjee *et al.* 2018), and it cannot reflect the increase in water demand because of temperature. In response to this limitation, Vicente-Serrano *et al.* (2010) introduced another widely used drought index, the Standardized Precipitation Evapotranspiration Index (SPEI). The SPEI uses the SPI's structure but applies temperature and P. This drought index can capture agricultural drought more efficiently than SPI can, as it uses potential evapotranspiration (ET_p) (Yihdego *et al.* 2019). However, the SPEI may face limitations when comparing drought across different climate regions (Mukherjee *et al.* 2018).

P is the basis for the calculation of many drought indices. At different time aggregations, P can help indicate all types of droughts. It is relatively the most direct variable of water supply (Yihdego *et al.* 2019; Slater *et al.* 2021). However, using only P leads to a failure to incorporate the changes in available energy, air humidity, and wind speed; consequently, it can provide values that do not capture reality (Mukherjee *et al.* 2018). Drought relies not only on water supply but also on water demand, for which ET can be the proxy (Speich 2019). ET forces around 60% of the land P to return to the atmosphere (Zhang *et al.* 2020) and creates two-thirds of the planet's annual P. It also consumes more than half of the solar energy absorbed by the land surface as latent heat. Accordingly, ET, which contributes to mass and energy exchange between land and atmosphere (Zhang *et al.* 2020; Hobeichi *et al.* 2021), is crucial in improving our vision of land–atmosphere interactions and the terrestrial water cycle (Zheng *et al.* 2019; Xiao *et al.* 2020). These explain ET's important role in releasing droughts (Mukherjee *et al.* 2018) and drought severity at both the local and global scales (Dhungel & Barber 2018; Zhang *et al.* 2020). Therefore, using ET together with P in the structure of drought indices allows for a more comprehensive drought assessment (Zargar *et al.* 2011; Lu *et al.* 2019).

ET has several types, and selecting its type is highly critical in defining the drought index. For instance, the so-called Standardized Precipitation Actual Evapotranspiration Index uses actual evapotranspiration (ET_a) in its structure (Homdee *et al.* 2016). However, the difference between P and ET_a could not capture the real water shortage (WS). This is because ET_a is not the ultimate possible amount of ET but the real ET occurring on the surface (Kim & Rhee 2016; Vicente-Serrano *et al.* 2018). As one of the other types of ET, ET_p, which has already been used in the structure of some drought indices in the literature, is a measure of atmospheric evaporative demand (Kim & Rhee 2016; Vicente-Serrano *et al.* 2018; Yihdego *et al.* 2019; Dash *et al.* 2021). Wet-environment evapotranspiration (ET_w) is ET from an extensive, well-watered surface into the atmosphere (Kahler & Brutsaert 2006).

To specify the appropriate water demand term for drought assessment, it is essential to be aware of both water balance and energy balance (Koppa *et al.* 2021). The literature in this area is rich, and among existing studies is the rigorous work conducted by Fisher *et al.* (2011), which has taken a proper look into the concept.

Based on water balance in a closed system (e.g., a watershed), where P is the only water supply, the supplied water takes one of the following forms (human systems, extraction by insects or animals, and leaking into the earth's deep crust are not part of this scope):

(1) Going into the soil and groundwater flow or recharge (GW); (2) surface runoff (R); (3) being stored in lakes, ponds, and plants (S); and (4) going back to the atmosphere (ET_a). The water balance equation is expressed as follows:

$$P = GW + R + S + ET_a \tag{1}$$

The upper limit of ET_a in water balance is ET_w and will occur only if enough water is supplied (Fisher *et al.* 2011). ET_w changes by energy variation. Then, we can define water loss via ET as follows:

$$P - ET_a = GW + R + S \tag{2}$$

Apparently, we always have $P - ET_a \geq P - ET_w$.

Then, one can claim that ET_w illustrates the real ET demand.

Despite its important role as an indicator of water demand, the use of ET_w in the structure of P-based drought indices has been almost overlooked in the literature. Incorporating ET_w in drought index calculations, especially for agricultural purposes, is advantageous. It captures a more realistic condition in which the important role of ET as water demand is neither underestimated nor overestimated by using a pessimistic indicator.

As a robust and generalized drought index running through a simple structure is essential for improving water resource management and planning (Yihdego *et al.* 2019), this research introduces the Wet-environment Evapotranspiration and Precipitation Standardized Index (WEPSI), in which water supply and demand are incorporated into the drought index calculation. WEPSI follows the SPI methodology for its calculation, while P is considered for water supply and ET_w for water demand. Priestley and Taylor's model (P–T model) (Priestley & Taylor 1972) is widely used as a proxy of ET_w (Kahler & Brutsaert 2006). This model has a coefficient that was proposed to account for the drying power of the air, with an estimated mean value of 1.26 (or $\alpha = 1.26$) over saturated surfaces, such as oceans. Recent research has shown that this coefficient is impacted by the radiation regime, relative humidity, air temperature, wind speed, and geographical site. This raises doubts about the use of P–T model outputs without calibration of its coefficient (Aminzadeh & Or 2014). Accordingly, we used an asymmetric Complementary Relationship (CR) to obtain ET_w using ET_a and ET_p, based on our reliable data (Khoshnazar *et al.* 2021a, 2021b). To evaluate the performance of WEPSI, we first compared its results with both well-known drought indices (SPI, SPEI), as well as with the Standardized Runoff Index (SRI). The coefficient of determination, root mean square error (RMSE), mean absolute deviation (MAD), and mutual information were used for this comparison. Additionally, the fluctuation in cereal yield and crop production in El Salvador, as well as El Niño Southern Oscillation (ENSO) events, was compared to drought calculated using WEPSI, illustrating its performance, especially for agricultural purposes. We assessed WEPSI at the catchment scale using ET data calculated from the Water Evaluation And Planning (WEAP) system hydrological model.

The remainder of the paper is organized as follows. In Section 2, Materials and Methods, we start with our case study area. Then, the WEAP model (Section 2.2), WEPSI (Section 2.3), and benchmark drought indices (Section 2.4) are described. Later, the experimental setup is presented (Section 2.5). The results and discussion are given in Section 3. Finally, Section 4 concludes the paper and suggests directions for future research.

2. MATERIALS AND METHODS

2.1. Case study

The transboundary Lempa River basin located in the Central American dry corridor is used as our case study area in investigating WEPSI. With a length of 422 km, the Lempa River is the longest stream in Central America. It originates from volcanic mountains in Guatemala, with 1,500 masl elevation, and flows to the Pacific Ocean in El Salvador. Around 360.2 km (85%) of the river's length flows into El Salvador's territory (Hernández 2005). This river flows through Guatemala, Honduras, and El Salvador (Figure 1). The area of the tri-national basin is 17,790 km^2, of which 10,082 km^2 belongs to El Salvador (49% of El Salvadorian land). The basin has a daily average temperature of 23.5 °C, a total annual rainfall average of 1,698 mm, and a yearly R of 19.21 $dm^3\ s^{-1}\ km^2$.

The Lempa River streamflow has dropped by 70% (Jennewein & Jones 2016; Helman & Tomlinson 2018) during the dry years. This is while based on El Salvador's Ministry of Environment & Natural Resources (MARN) (2019b) data, El Salvador gains 68% of its surface water from this river basin. The basin environs 13 of 14 departments of El Salvador, including 3,967,159 inhabitants (77.5% of the country's population). Alterations in the hydrological regime, such as extreme events (e.g., drought and tropical cyclone), worsen water quality and quantity in the region (Global Environment Facility 2019). The current condition of the basin highlights the need for water resource management and drought assessment.

2.2. The WEAP model

The WEAP system is a well-known model for water resource planning developed by the Stockholm Environment Institute (Seiber & Purkey 2015). WEAP allows the calculation of terrestrial hydrological cycle variables, such as R, infiltration, and ET. We used WEAP-derived ET to calculate WEPSI. The required input data on hydrometeorological and soil characteristics of the model were obtained from MARN (2019a), and the updated version of Sheffield *et al.* (2006) for the period 1980–2010. Based on basin management by local authorities and physiographic characteristics, the Lempa River basin

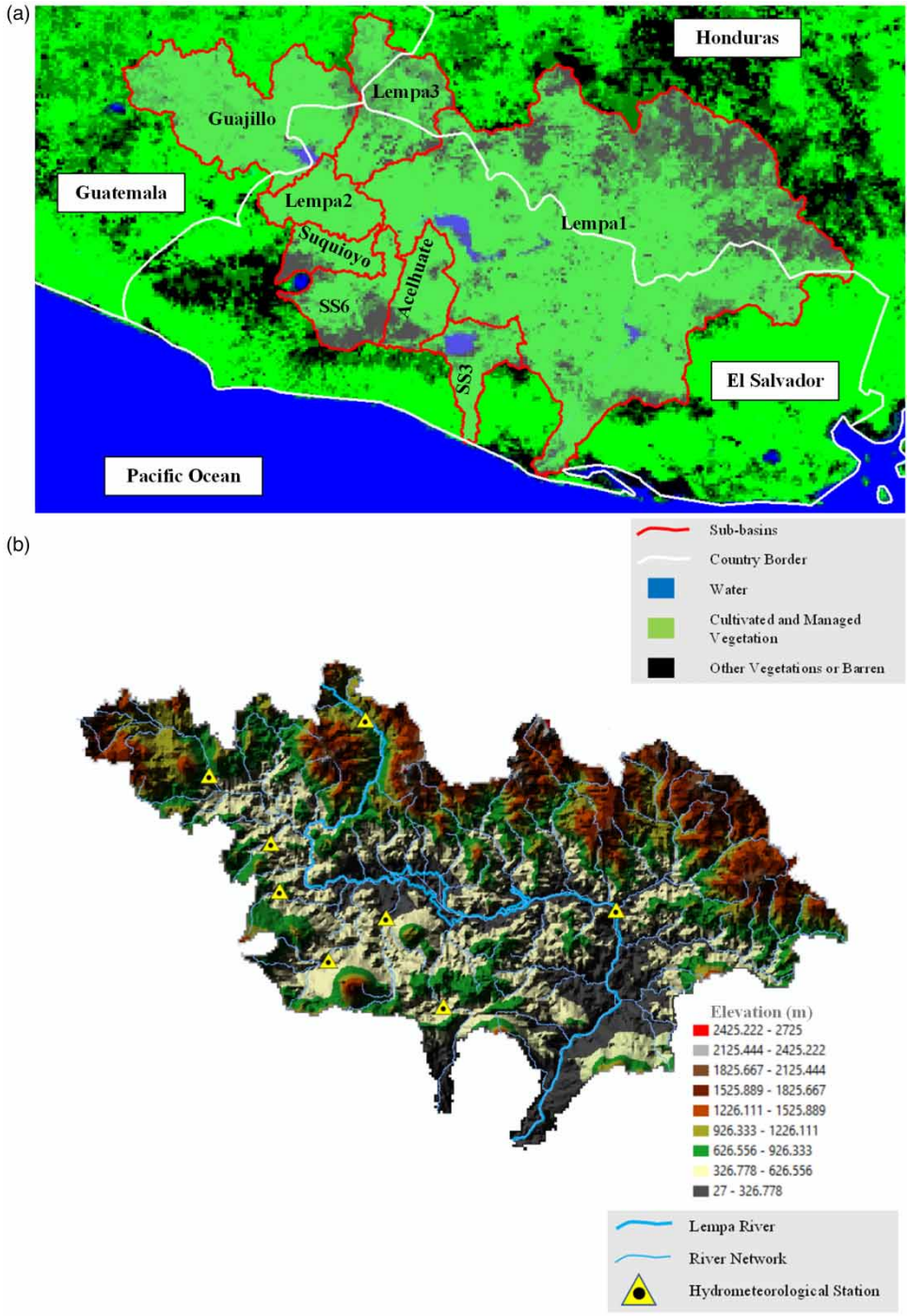

Figure 1 | The Lempa River basin: (a) location, and cultivated and managed vegetation and (b) drainage basin.

was divided into the following eight sub-basins: Lempa 1, Lempa 2, Lempa 3, Guajillo, Suquioyo, Acelhuate, SS6, and SS3 (Figure 1). Khoshnazar *et al.* (2021a, 2021b) showed that the WEAP-derived variables are reliable for drought assessment in the Lempa River basin. For the description of the validation and calibration procedure of the model, interested readers are referred to our previous publication (Khoshnazar *et al.* 2021a, 2021b).

Five methods to simulate basin processes, such as ET, R, and irrigation demands, are available in WEAP. In our research, we use the soil moisture method, which considers that the basin has two soil layers (buckets or tanks). The top soil layer is

considered shallow-water capacity, and the bottom soil layer is considered deep-water capacity. Figure 2 depicts a conceptual diagram of the soil moisture method (Seiber & Purkey 2015). The water balance is calculated for each fraction area j for the first layer, assuming that the climate is steady in each sub-basin. The water balance is calculated using Equation (3) as follows (Oti *et al.* 2020):

$$\mathrm{Rd}_j \frac{\mathrm{dZ}_{1,j}}{\mathrm{d}t} = \mathrm{P_e}(t) - \mathrm{ET_p}(t) k_{c,j}(t) \left(\frac{5\mathrm{Z}_{1,j} - 2\mathrm{Z}_{1,j}^2}{3} \right) - \mathrm{P_e}(t) \mathrm{Z}_{1,j}^{\mathrm{RRF_j}} - f_j k_{s,j} \mathrm{Z}_{1,j}^2 - (1 - f_j) k_{s,j} \mathrm{Z}_{1,j}^2 \quad (3)$$

where $Z_{1,j}$ is the relative storage based on the total effective storage of the root zone. Rd_j is the soil holding capacity of the land cover fraction j (mm). $\mathrm{ET_p}$ is calculated using the modified Penman–Monteith reference crop $\mathrm{ET_p}$ with the crop/plant coefficient ($k_{c,j}$). $\mathrm{P_e}$ is the effective precipitation (P), and RRF_j is the R resistance factor of the land cover. $\mathrm{P_e}(t)\mathrm{Z}_{1,j}^{\mathrm{RRF}_j}$ is indicated as the surface R. $f_j k_{s,j} \mathrm{Z}_{1,j}^2$ shows the interflow from the first layer, for which the term $k_{s,j}$ denotes the root zone saturated conductivity (mm/time), and f_j is the partitioning coefficient that considers water horizontally and vertically based on the soil, land cover, and topography. Finally, the term $(1 - f_j) k_{s,j} \mathrm{Z}_{1,j}^2$ is percolation. WEAP uses Equation (4) to calculate $\mathrm{ET_a}$ (Kumar *et al.* 2018):

$$\mathrm{ET_a} = \mathrm{ET_p} \frac{(5z_1 - 2z_2^2)}{3} \quad (4)$$

where z_1 and z_2 are the water depth of the top and bottom soil layers (bucket), respectively (Figure 2).

For the drought analysis, we calculated the monthly $\mathrm{ET_w}$ with the WEAP-derived $\mathrm{ET_p}$ and $\mathrm{ET_a}$ following the procedure presented in Section 2.3.2.

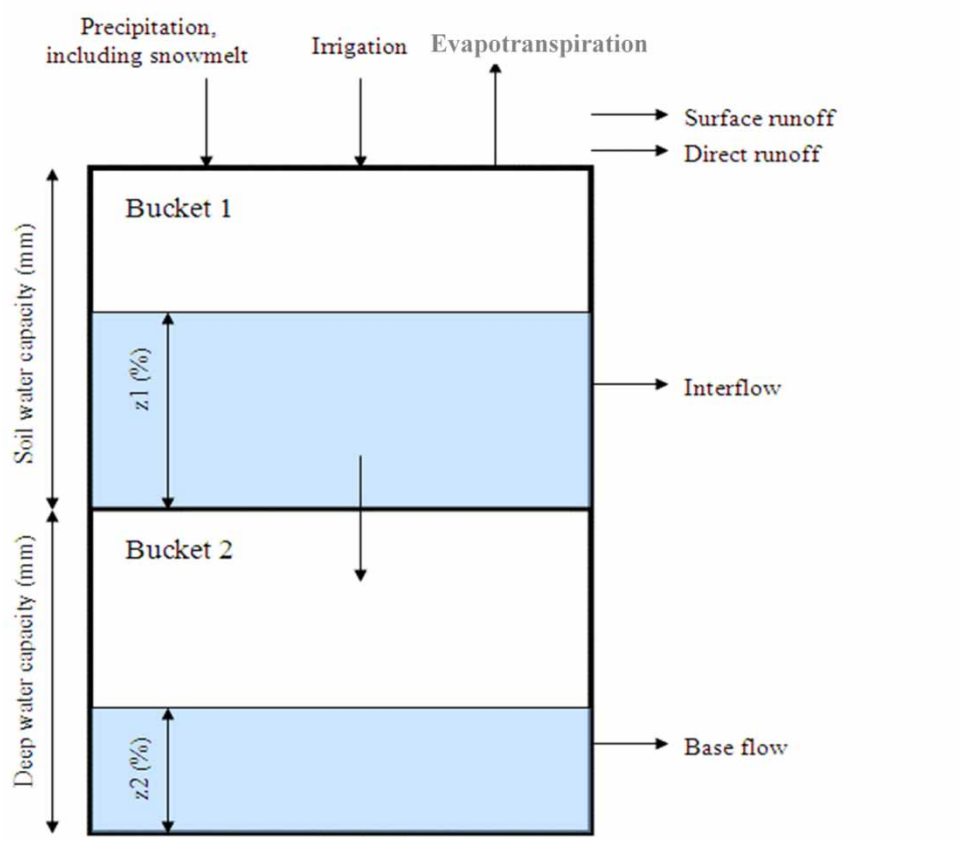

Figure 2 | Conceptual diagram of the water balance calculation in WEAP, after Seiber & Purkey (2015).

2.3. The WEPSI

2.3.1. WEPSI calculation

WEPSI is calculated following the SPI methodology (Section 2.4.1) to standardize the input, except that WEPSI uses WS instead of P alone.

WS is calculated as the difference between P (water supply) and ET_w (water demand) (Equation (5)).

$$WS = P - ET_w \tag{5}$$

WEPSI is inspired by the structure of the SPEI that uses ET_p to incorporate water demand into the drought index calculation. Based on our discussions in the previous section, ET_w can be an appropriate representative of water demand. Accordingly, we incorporate ET_w into WEPSI as the water demand indicator and P to account for the water supply. Since WEPSI incorporates $P - ET_w$ as its input and concerning the water balance equation (Equation (1)), we anticipate that our proposed drought index should have a higher correlation with SRI and, therefore, can provide useful information about the hydrological situation of the area. We will later investigate this in the numerical results.

As LL3 distribution has shown good performance in SPEI calculation and similar drought indices, we consider LL3 distribution to fit WS in WEPSI calculation (Vicente-Serrano *et al.* 2010; Kim & Rhee 2016). Similar to SPI, WEPSI can be obtained based on different time steps, such as 3, 6, 9, 12, 24, and 48 months.

Since WEPSI follows the structure of the SPI, we consider the same drought categorical classification (Table 1).

ET_w used in Equation (5) is calculated based on the methodology introduced in the following subsection.

2.3.2. ET_w calculation

As previously mentioned, we have used CR to obtain ET_w data. Based on the Bouchet hypothesis (Bouchet 1963), equilibrium evapotranspiration or ET_w is equal to ET_a and ET_p under saturated conditions. A saturated condition refers to an extensive, well-watered surface where input energy is the limiting factor (Xiao *et al.* 2020). We always have $ET_a \leq ET_w$ and $ET_p \geq ET_w$. ET_w, ET_p, and ET_a have been related to one another by what is known as CR. A general form for CR is suggested by Kahler & Brutsaert (2006) (Equation (6)).

$$(1 + b)ET_w = bET_a + ET_p \tag{6}$$

where b is an empirical constant, and ET_a, ET_p, and ET_w are the actual, potential, and wet-environment evapotranspiration, respectively.

The symmetric CR considered by Bouchet is obtained by taking $b = 1$ in Equation (6). However, the literature indicates that b generally exceeds and is rarely equal to 1 (i.e., CR is asymmetric) (Aminzadeh *et al.* 2016). Consequently, for the ET_w calculation, in addition to ET_p and ET_a, it is necessary to estimate the value of b.

Equation (6) can be rewritten in terms of b (Aminzadeh *et al.* 2016).

$$b = \frac{ET_p - ET_w}{ET_w - ET_a} \tag{7}$$

Table 1 | Drought categorical classification using WEPSI

WEPSI value	Drought/Wet category
≥2	Extreme wet
1.5–2	Severe wet
1–1.5	Moderate wet
0–1	Low wet
−1 to 0	Low drought
−1.5 to −1	Moderate drought
−2 to −1.5	Severe drought
≤− 2	Extreme drought

Equation (7) shows that the increase in ET_p above ET_w is proportional to the energy flux provided by surface drying and the decrease in evaporation rate.

Normalizing Equation (7) results in Equations (8) and (9) (Aminzadeh *et al.* 2016),

$$ET_{a+} = \frac{(1+b)ET_{MI}}{1+bET_{MI}} \tag{8}$$

$$ET_{p+} = \frac{1+b}{1+bET_{MI}} \tag{9}$$

where $ET_{a+} = ET_a/ET_w$, $ET_{p+} = ET_p/ET_w$, $ET_{MI} = ET_a/ET_p$, and ET_{MI} is the surface moisture index (with a maximum of 1). ET_{a+} and ET_{p+} are the scaled actual and ET_p, respectively. Figure 3 illustrates the variation in the scaled actual and potential evapotranspiration with respect to different values of the surface moisture index.

The b parameter in Equations (8) and (9) can be obtained from Equation (10) (Granger 1989; Aminzadeh *et al.* 2016; Xiao *et al.* 2020),

$$b = \frac{1}{\gamma}\frac{e_s^* - e_w^*}{T_s - T_w} \tag{10}$$

where e_s^* is the saturated vapor pressure at surface temperature T_s, and e_w^* is the saturated vapor pressure at a hypothetical wet surface temperature T_w. The psychometric constant γ (in k Pa $^\circ C^{-1}$) is calculated with the atmospheric pressure (Pe) as $\gamma = 0.665 \times 10^{-3}$Pe, with Pe in kPa.

Alternatively, to facilitate the calculation of CR, Aminzadeh *et al.* (2016) suggested an atmospheric input-based equation for b (Equation (11)), which is more straightforward than Equation (10) (Han & Tian 2020); this is why we have used this equation in our paper.

$$b = A\, R_{S,\ net} + B \tag{11}$$

where $R_{S,\ net}$ is the net shortwave radiation flux in W m^{-2}. $R_{S,net}$ is calculated with the incoming shortwave radiation flux R_S and the surface albedo α as $R_{S,\ net} = (1-\alpha)R_s$.

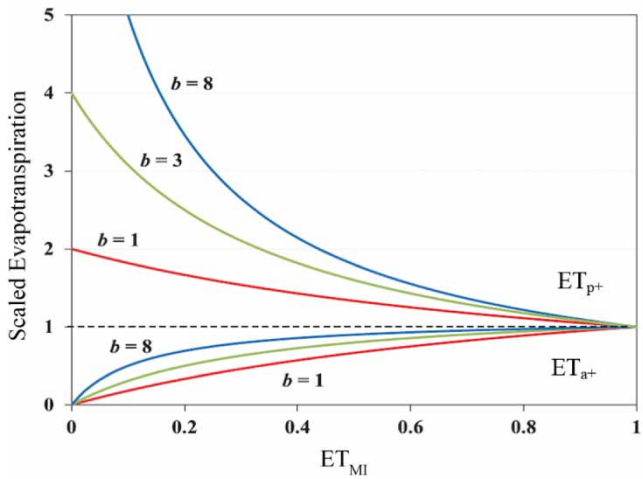

Figure 3 | Scaled actual (ET_{a+}) and potential evapotranspiration (ET_{p+}) with respect to the surface moisture index (ET_{MI}) variations for different values of b (Kahler & Brutsaert 2006; Aminzadeh *et al.* 2016).

A is a function of wind speed u_a (in m S^{-1}) (Equation (12)).

$$A = (3u_a + 2) \times 10^{-3} \tag{12}$$

Finally, the B parameter is calculated as a function of wind speed (u_a) and vapor concentration (c_a(kg m^{-3})) (Equation (13)).

$$B = (24.3\ u_a - 1.44)(c_a + 22 \times 10^{-3}) + 0.3 \tag{13}$$

To calculate b using Equation (11), $R_{S,\,net}$, u_a, and c_a are required, which can be obtained from meteorological measurements, the literature, or empirical equations.

2.4. Drought indices for comparison

We compare SPI (McKee *et al.* 1993) and SPEI (Vicente-Serrano *et al.* 2010) drought indices with WEPSI. As discussed, SPI is based on the total amount of water (i.e., P), whereas SPEI incorporates the reduction of water based on ET_p. We also include SRI (Shukla & Wood 2008) in the comparison. SRI is a hydrological drought index that reflects the real water availability on land. The application of the hydrological drought index can provide us with further insights into the situation of the studied area compared with using only meteorological drought indices (Shukla & Wood 2008). SRI implicitly reflects ET_a (Vicente-Serrano *et al.* 2010). Accordingly, when a meteorological drought index reflects a high similarity with SRI, it provides more insights into the hydrological situation of the land and is closer to the real evapotranspiration condition. Such an index has a higher potential to be used solely without requiring a complementary hydrological index and, consequently, eliminates the difficulty of gathering and modeling hydrological data.

The methodology for calculating the SPI, SPEI, and SRI drought indices is as follows.

2.4.1. The SPI

The methodology for calculating the SPI is presented as follows (McKee *et al.* 1993). Based on long-term P data (30 years or more), a time scale (also known as aggregation period) is specified. This time scale can be 3, 6, 9, 12, 24, or 48 months. Then, the aggregated P is fitted to a distribution function. Afterward, the cumulative probability function is equal to that of the normal distribution, for which the standardized variable with zero mean and unity standard deviation is obtained. The literature suggests the Gamma distribution as one of the best choices for SPI calculation (McKee *et al.* 1993; Kim *et al.* 2019). Therefore, we have used Gamma distribution for SPI calculation.

2.4.2. The SPEI

The SPEI follows the SPI methodology but uses the difference between P and ET_p as its input (Vicente-Serrano *et al.* 2010). Several studies have shown that the log-logistic distribution is appropriate for SPEI calculation (Vicente-Serrano *et al.* 2010). Accordingly, we have used the three-parameter log-logistic (LL3) distribution for obtaining the SPEI.

2.4.3. The SRI

The SRI uses runoff (R) as input and follows a similar procedure as SPI (Shukla & Wood 2008). McKee *et al.* (1993) proposed a gamma distribution for the SPI and suggested that this distribution is operational for other variables related to drought (Sorí *et al.* 2020). Accordingly, we have used the Gamma distribution to calculate SRI, utilizing R data obtained from the WEAP model.

2.5. Experimental setup

2.5.1. WEPSI calculation at the catchment scale

WEPSI is applied in the Lempa River basin; we have calculated it for each sub-basin (Section 2.1). Equation (6) is used to obtain ET_w.

To derive ET_w from Equation (6), we first applied Equation (11) to calculate parameter b for 12 months of the year in each sub-basin. In this order, the daily datasets of wind speed (u_a), net shortwave radiation ($R_{S,\,net}$), and vapor concentration (c_a) for 31 years (1980–2010) and for each sub-basin are used to calculate the monthly average of these three inputs. The

meteorological data u_a, $R_{S,\,net}$, and c_a were retrieved from MARN (2019a) and Khoshnazar *et al.* (2021a, 2021b). The ranges of the obtained b values are validated by comparing them with the values available in the literature (Aminzadeh *et al.* 2016).

After obtaining b, we used the time series of WEAP-derived ET_p and ET_a (Section 2.2) as the inputs of Equation (6) to calculate ET_w in each sub-basin.

Finally, with the catchment-wide P and ET_w, we computed WEPSI for the time steps 3, 6, 9, and 12 months, which are indicated as WEPSI03, WEPSI06, WEPSI09, and WEPSI12, respectively.

2.5.2. WEPSI performance evaluation

To compare WEPSI in calculating drought, we have used SPI and SPEI, two vastly applied meteorological drought indices. In drought studies, the SPEI has also been applied to agricultural drought assessments. We further utilized the SRI as a hydrological drought index to investigate whether WEPSI could provide insights into the hydrological situation. For the calculation of the SPI, SPEI, and SRI, we followed the methodology presented in Section 2.4. The catchment-wide P, ET_p, and R derived from the WEAP model were the inputs used to compute the drought indices for each sub-basin. These three drought indices were similarly calculated for the time steps 3, 6, 9, and 12 months. The same notation used in WEPSI is utilized in this case. Therefore, for instance, the 6-month time step for the SPI, SPEI, and SRI is indicated as SPI06, SPEI06, and SRI06, respectively.

The comparison is carried out in the following steps. First, three metrics commonly used in the performance evaluation of drought indices are applied to compare WEPSI, SPI, SPEI, and SRI, which are the coefficient of determination (r^2), RMSE, and, MAD. These metrics are calculated using Equations (14)–(16), respectively, as follows (Mahmoodzadeh *et al.* 2022; Pant & Kumar 2022):

$$r^2 = \left(\frac{\sum_{i=1}^{n} (x_i - \bar{x})(y_i - \bar{y})}{\sqrt{\sum_{i=1}^{n} (x_i - \bar{x})^2 \sum_{i=1}^{n} (y_i - \bar{y})^2}} \right)^2 \tag{14}$$

$$\mathrm{RMSE} = \sqrt{\left(\frac{1}{n}\right) \sum_{i=1}^{n} (x_i - y_i)^2} \tag{15}$$

$$\mathrm{MAD} = \frac{1}{n} \sum_{i=1}^{n} |x_i - y_i| \tag{16}$$

where x_i and y_i indicate the reference variable and the variable to compare, respectively, and $\bar{x}$ and $\bar{y}$ indicate the mean of such values.

Second, we use the concept of mutual information (MI) to complement our evaluation, where MI is calculated between WEPSI, SPI, SPEI, and SRI. MI is calculated between two variables to determine the amount of information one variable has about the other (Vergara & Estévez 2014). This concept is valuable in our comparison procedure, as we seek to know how much information is available about the others in each drought index. MI is calculated using Equation (17) (interested readers are referred to Vergara & Estévez (2014) and Al Balasmeh *et al.* (2020) for the theoretical background underlying the calculation of MI).

$$\mathrm{MI}(x; y) = \mathrm{H}(x) - \mathrm{H}(x|y) = \sum_{i=1}^{n} \sum_{j=1}^{n} p(x(i),\ y(j)) \cdot \log\left(\frac{p(x(i),\ y(j))}{p(x(i)) \cdot\ p(y(j))} \right) \tag{17}$$

where $\mathrm{MI}(x; y)$ is the MI between variables x and y, $\mathrm{H}(x)$ is the entropy of a discrete random variable x, $\mathrm{H}(x|y)$ is the conditional entropy of two discrete random variables of x and y, $p(x)$ denotes the probability of the random variable x, and $p(x,\ y)$ is the joint probability of the random variables of x and y. MI is zero if x and y are statistically independent, and $\mathrm{MI}(x; y) = \mathrm{MI}(y; x)$.

The unit of information or entropy is nat (natural unit of information), which is based on natural logarithms and powers of e instead of the base two logarithms and powers of two used in the bit unit.

Figure 4 shows the Venn diagram based on Equation (17), which schematizes the relationship between MI and entropies (H) between the random variables x and y.

As drought is an important environmental driver that leads to cereal loss in both yield and quality worldwide (Karim & Rahman 2015; Warter *et al.* 2021), we also compare the cereal yield data of El Salvador with the results of the drought indices in this research.

With the time series of WEAP-based WEPSI calculated in each sub-basin, we compute the time series of the percentage of drought area (PDA) for the entire basin. PDAs were calculated monthly as the ratio between the area of sub-basins in drought and the total area of the basin. A drought event starts once the drought index value goes below a threshold and ends as the value rises above the threshold again (Corzo Perez *et al.* 2011; Brito *et al.* 2018; Corzo *et al.* 2018; Diaz *et al.* 2020). The threshold used in this application was drought index $= -1$, which is a threshold commonly used in drought assessments (Diaz *et al.* 2020; Khoshnazar *et al.* 2021a, 2021b).

Finally, we compared PDA fluctuations with El Niño–La Niña years and with El Salvadorian cereal yield. Cereal yield is used because a lack of soil moisture can lead to a severe reduction in cereal yield. On the other hand, drought causes yield and quality loss of cereal globally. Then, if WS, and thereby WEPSI, can capture the status of soil moisture and drought, there should exist a relationship between WEPSI and cereal yield (Lewis *et al.* 1998; Khoshnazar *et al.* 2021a, 2021b).

3. RESULTS AND DISCUSSION

3.1. WEPSI calculation and performance evaluation

About the input variables for WEPSI, we have the following. CR was used to calculate the ET_w dataset as follows. The b parameter was calculated following the methodology presented in Section 2.3.2 for 12 months in eight sub-basins. Figure 5 depicts the asymmetric CR between ET_{a+} and ET_{p+} as functions of ET_{MI} for 12 months of the year in the Guajillo sub-basin. This figure also shows the symmetric CR that would occur if b was equal to 1. As Figure 5 illustrates, compared with the symmetric CR, the calculated b leads to a considerable difference between the scaled evapotranspiration (ET_{a+} and ET_{p+}) as the surface dries and ET_a decreases (Aminzadeh *et al.* 2016).

Figure 5 also highlights the importance of using local and temporal meteorological data (net shortwave radiation, wind speed, and vapor concentration), which can lead to a more accurate approximation of CR and, consequently, of ET_w.

Figure 6 shows the time series of SPI06, SPEI06, SRI06, and WEPSI06 in the Guajillo sub-basin as an example of the calculation of the drought indices.

Our results show that in 61% of the cases, the value of WEPSI06 is larger than that of SPEI06, i.e., SPEI depicts a worse situation than WEPSI. The findings indicate that this behavior of WEPSI is also observed among all other sub-basins.

The literature states that an SPI with 3- or 6-month steps can be considered as an agricultural drought index (McKee *et al.* 1993; Vicente-Serrano 2006; Khoshnazar *et al.* 2021a, 2021b). It is also shown that SPI and SPEI, with 6-month time steps, have the highest correlation with each other (Diaz Mercado *et al.* 2018). Additionally, we compared the river streamflow with WEPSI and SRI for 3-, 6-, 9-, and 12-month time steps. We found that WEPSI06 and SRI06 were most related in terms of low flow in the basin. Accordingly, we consider WEPSI06 representative of the agricultural and hydrological drought conditions

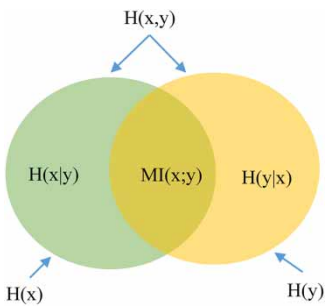

Figure 4 | The Venn diagram of the relationship between mutual information (MI) and entropy (H).

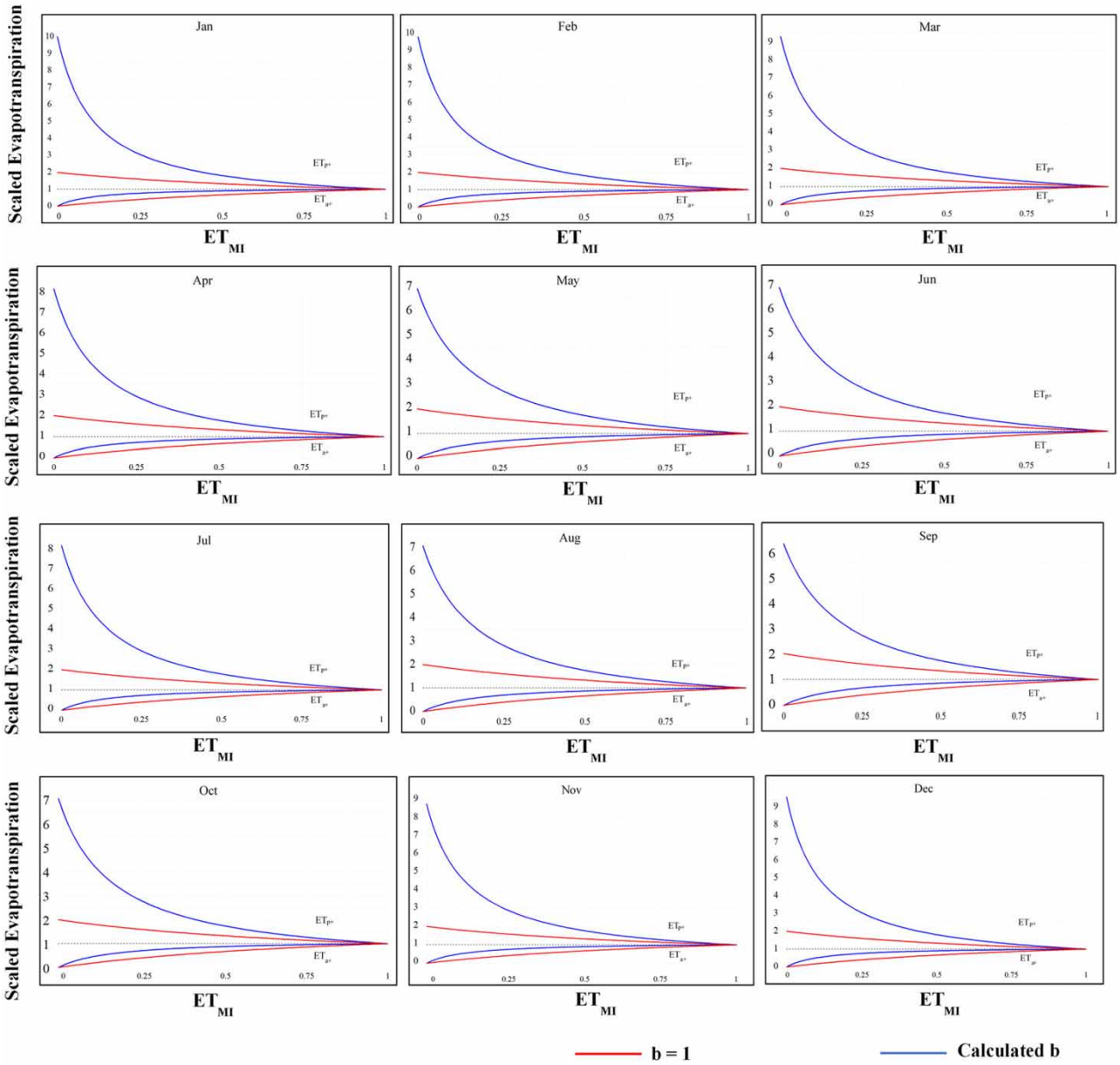

Figure 5 | Scaled actual (ET_{a+}) and potential evapotranspiration (ET_{p+}) with respect to the surface moisture index (ET_{MI}) in the Guajillo sub-basin for 12 months of the year.

in the basin – WEPSI06 reflected a realistic vision of the basin that links meteorological, agricultural, and hydrological drought.

The correlation, RMSE, and MAD between the four drought indices are presented in Table 2. Values presented in Table 2 are the averages of the three metrics of the eight sub-basins. The correlations between WEPSI06 and SPI06 (0.931), WEPSI06 and SPEI06 (0.904), and WEPSI06 and SRI06 (0.783) are the highest. In comparison with the other drought indices, WEPSI has the highest correlation with all drought indices, and the correlation between SPEI06 and SRI06 (0.501) is the lowest. In opposite, the RMSE and MAD values show the lowest values between WEPSI06 and SPI06, WEPSI06 and SPEI06, and WEPSI06 and SRI06, for both metrics. As Table 2 shows, the highest amounts of RMSE and MAD are between SPEI and SRI. It is noteworthy that, higher values of r^2 show that the pattern of changes are more similar. On the other hand, lower values of RMSE and MAD indicate that the deviation of two datasets is smaller.

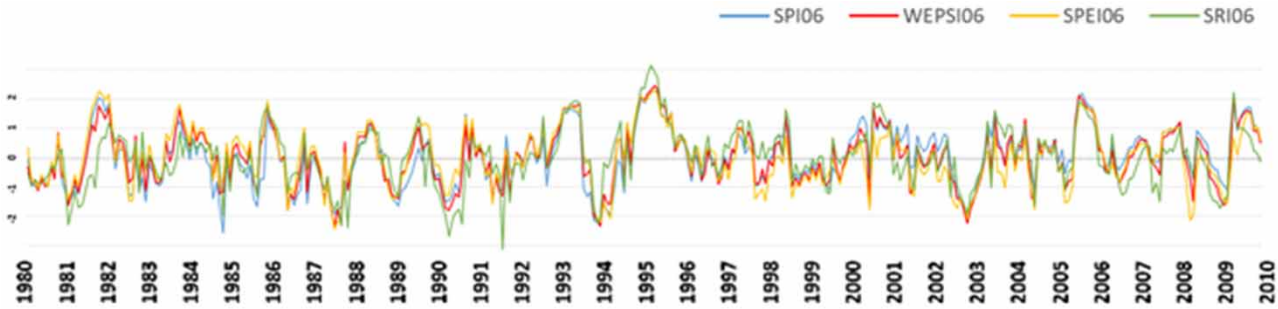

Figure 6 | SPI06, SPEI06, SRI06, and WEPSI06 time series based on the WEAP-derived ET data for the Guajillo sub-basin (1980–2010).

Table 2 | Statistical metrics between drought indices

		Drought indices			
Drought indices	**Metric**	**SPI06**	**SPEI06**	**SRI06**	**WEPSI06**
SPI06	r^2	1	0.741	0.634	0.931
	RMSE	0	0.550	0.697	0.358
	MAD	0	0.421	0.545	0.268
SPEI06	r^2	0.741	1	0.501	0.904
	RMSE	0.550	0	0.779	0.402
	MAD	0.421	0	0.603	0.304
SRI06	r^2	0.634	0.501	1	0.783
	RMSE	0.697	0.779	0	0.530
	MAD	0.545	0.603	0	0.419
WEPSI06	r^2	0.931	0.904	0.783	1
	RMSE	0.358	0.402	0.530	0
	MAD	0.358	0.304	0.419	0

In addition to the aforementioned statistic metrics, MI was calculated among the drought indices (Section 2.5.2). As mentioned, MI was calculated to identify which drought index contains more information about the others. MI is expressed in nat, the International System of Units' unit for entropy (details in Section 2.5.2). Figure 7 depicts Venn diagrams that provide MI between drought indices. The values presented in Figure 7 are the averages of the eight sub-basins.

Our results are in line with the findings of Qaisrani *et al.* (2022), in Pakistan, indicating that the results of a drought index which takes temperature data and precipitation into account are more reliable than SPI, and showing that SPI is not much effective for the correlation of agricultural production.

The highest MI is between WEPSI06 and SPI06, WEPSI06 and SPEI06, and WEPSI06 and SRI06, with 0.74, 0.69, and 0.54 nat, respectively. The lowest MI is observed between SPEI06 and SRI06 (0.18 nat). The MIs between SPI06 and SPEI06, and SPI06 and SRI06 are 0.31 and 0.24 nat, respectively. Accordingly, WEPSI06 not only contains the highest amount of information about the two other meteorological drought indices (SPI06 and SPEI06) but also covers the most information about the hydrological conditions of the region (SRI06). SPEI06 and SPI06 send the lowest number of hydrological signals in terms of drought. The results of r^2, RMSE, MAD, and MI suggest that WEPSI is a drought index that identifies hydrological drought in the absence of R data.

Figure 8(a)–8(h) compares the time series of the WEAP-based WEPSI06 in the eight sub-basins of the Lempa River basin for the period 1980–2010 (31 years). Based on Figure 8, the longest drought (i.e., number of months in which the value of WEPSI is below the threshold of −1) occurred in 2003, in general. The maximum drought frequency (3.54%) occurred in the Guajillo, SS6, and Suquioyo sub-basins, with a total of 13 droughts over 31 years. The most severe drought (i.e., aggregation of WEPSI values in sequent months at drought) occurred in Guajillo in December 1994.

Figure 9 displays the variation of drought areas through the PDAs in the Lempa River basin for 31 years based on WEPSI06. The threshold of −1 was used to calculate drought in each WEPSI time series (i.e., a sub-basin is in drought if

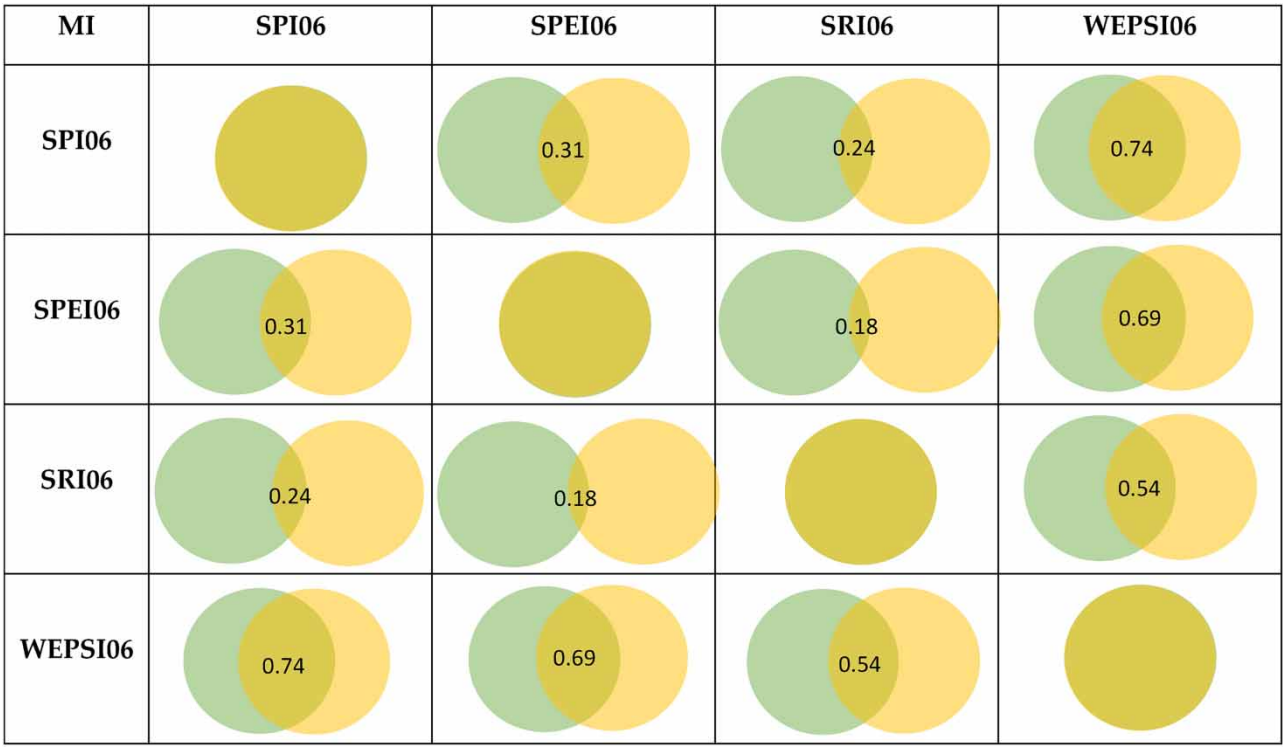

Figure 7 | Mutual information (MI) Venn diagram between SPI06, SPEI06, SRI06, and WEPSI06. The intersection between two circles depicts the MI between two drought indices in nat, the SI unit for entropy.

WEPSI06 ≤ -1; Table 1). Figure 9 shows some repetitive patterns in the behavior of droughts in the basin. Some years are in white cells, indicating the absence of PDA in those years, which are known as white years. By contrast, some other years show a tail (i.e., PDA occurs in some sequenced months, indicating long drought events).

As ENSO events are usually linked to major flood and drought episodes (Mera *et al.* 2018), we have applied this information to assess the performance of WEPSI. Drought events indicated by the PDA results (Figure 9) are compared with the EL Niño and La Niña years based on the Oceanic Niño Index (ONI) (National Oceanic & Atmospheric Administration 2015). ENSO events affect people and ecosystems across the globe via the production of secondary results that influence food supplies and prices, as well as forest fires, and create additional economic and political consequences (National Oceanic & Atmospheric Administration 2015). Comparing the patterns of PDA based on WEPSI06 (Figure 9) and the ONI shows that PDA shares similarities with La Niña in terms of white years, including weak La Niña in 1984, 2001, 2005, and 2006, moderate La Niña in 1995, 1996, 2000, and 2008, and strong La Niña in 1999. On the other hand, investigating the years with a drought tail reveals weak El Niño in 1980, 2004, 2007, 2009, and 2010, moderate El Niño in 1986, 1994, 2002, and 2003, strong El Niño in 1987, 1988, 1991, and 1992, and very strong El Niño in 1998. The consistency of the results provided by WEPSI06 with El Niño and La Niña years emphasize the good performance of WEPSI.

The fluctuation in cereal yield (kg per hectare) and the crop production index in El Salvador is shown in Figure 10 for the period 1980–2010 (31 years), we used data prepared by the Food and Agriculture Organization of the United Nations (FAO) (The World Bank Group 2021). Cereal yield, measured as kilograms per hectare of harvested land, includes wheat, rice, maize, barley, oats, rye, millet, sorghum, buckwheat, and mixed grains. The crop production index shown in Figure 10, depicts agricultural production for each year relative to the base period 2014–2016, including all crops except fodder crops (interested readers are referred to The World Bank Group (2022), for more details about how this index is calculated).

As Figure 10 depicts, in 1984, 1988, 1992, 1995, 1999, 2002, 2006, and 2008, cereal yield presented the local maximum amount compared with that in previous and subsequent years or cereal yield is ascending compared with the previous year. On the other hand, the years 1982, 1986, 1991, 1994, 1997, 2001, 2003, and 2007 presented the local minimum or cereal yield is descending compared with the previous year. These years with the local minimum and maximum, aside

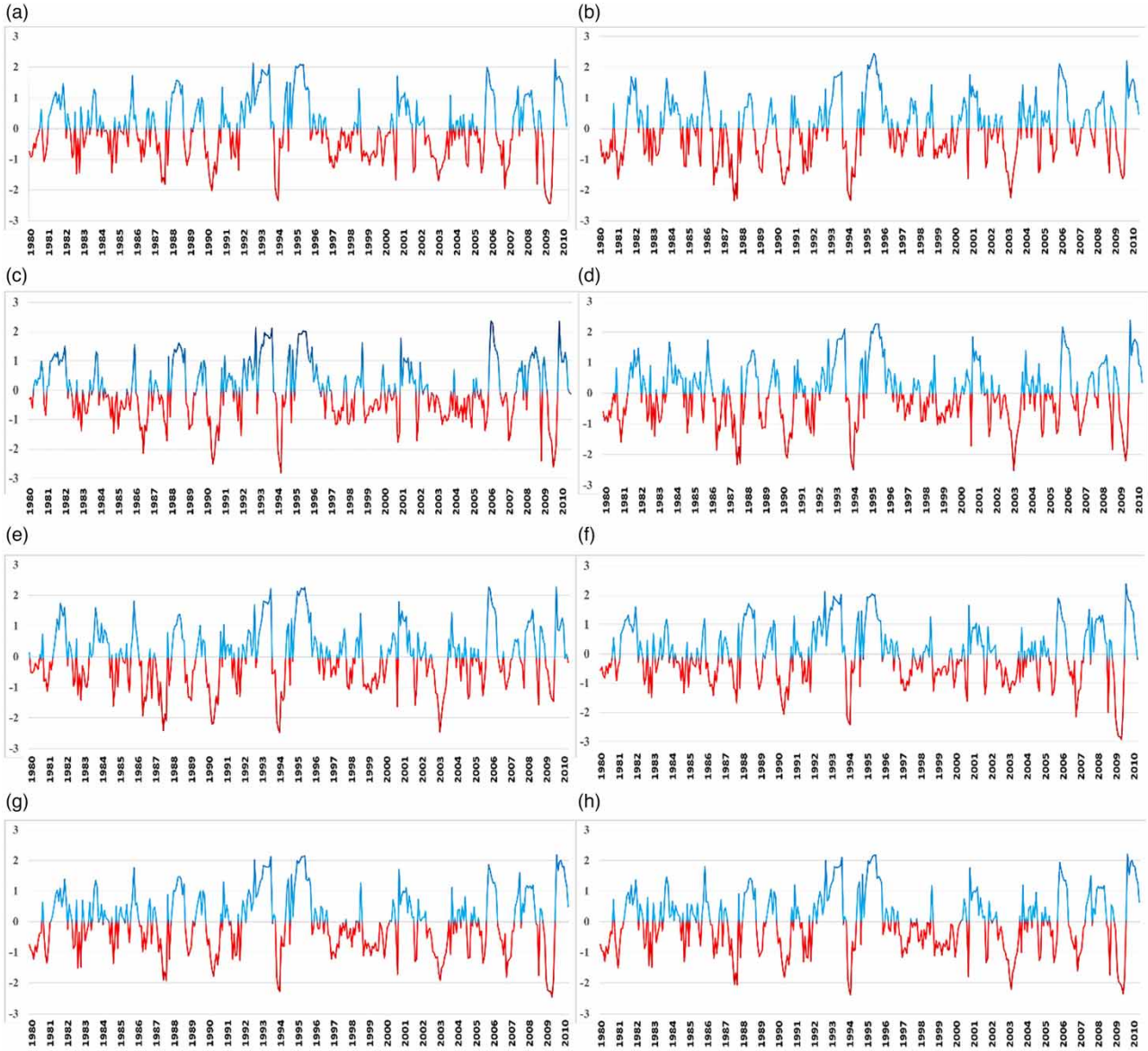

Figure 8 | Time series of WEPSI06 in the sub-basins: (a) Acelhuate, (b) Guajillo, (c) Lempa 1, (d) Lempa 2, (e) Lempa 3, (f) SS3, (g) SS6, and (h) Suquioyo.

from the years with descending and ascending cereal yield amounts (compared with the previous year), were used for the comparison with drought indices' PDA. Our results endorse that the PDA of WEPSI06 based on the WEAP model data detects six of the nine local maximums in El Salvador's cereal yield evolution (when a year does not have at least two sequent months with a PDA value greater than 0% based on the drought index, and that year has a local maximum in the cereal yield graph, the drought index is detecting the local maximum of cereal yield), as well as six of the nine local minimums in cereal yield fluctuation (when a year has some consecutive months with a PDA value greater than 0% based on the drought index, and that year has a local minimum in the cereal yield graph, the drought index is detecting the local minimum of cereal yield). It should be noted that since the PDA is calculated at the sub-basin level (details in the methodology section), when PDA is greater than 0% it means that at least one of the eight sub-basins is in drought. In addition, since the land cover of the basin is mostly agricultural (Figure 1), we assume that the drought area is a good proxy for agricultural drought.

This is while both SRI06 and SPEI06 detect four of the nine local maximums. SRI06 identifies five of the nine and SPEI06 reflects four of the nine local minimums of the graph. Finally, SPI06 does not detect a considerable number of critical points

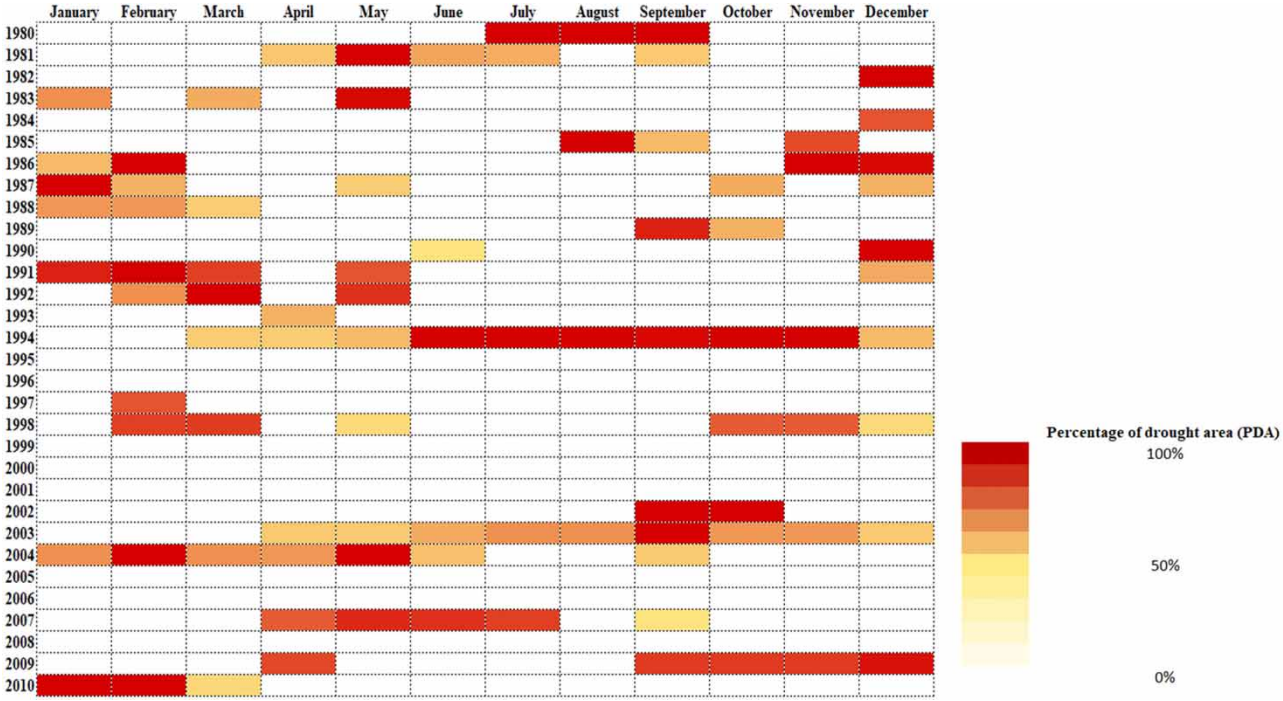

Figure 9 | Percentage of drought area (PDA) using WEPSI06 based on WEAP data in the Lempa River basin for the period 1980–2010.

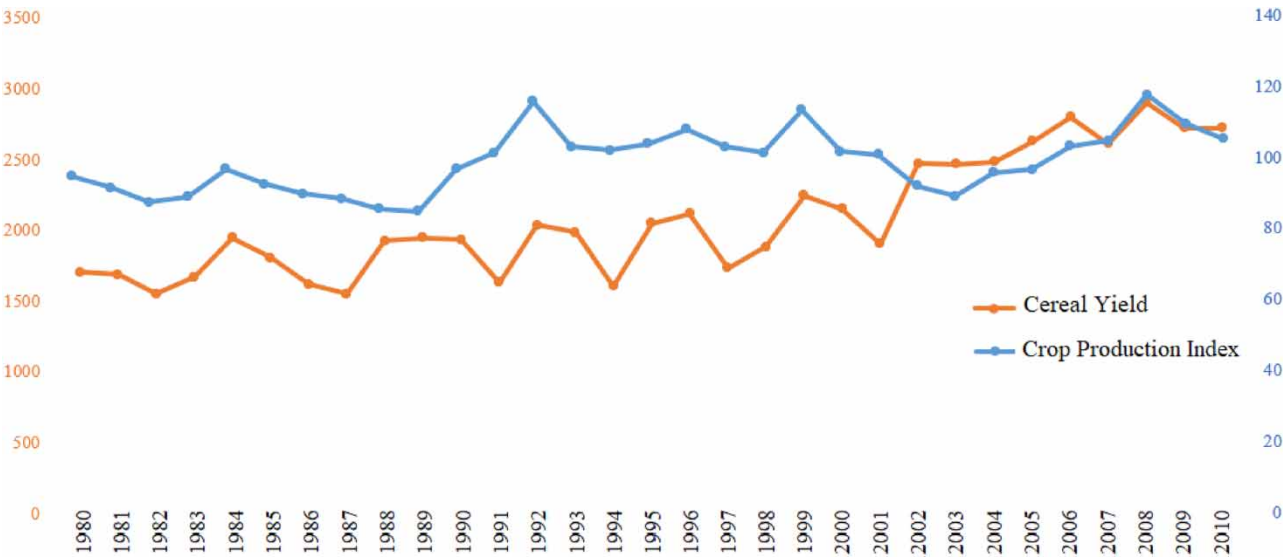

Figure 10 | Cereal yield (kg per hectare) and the crop production index in El Salvador for the period 1980–2010 (31 years).

(i.e., the local maximum and minimum points) in El Salvador's cereal yield graph. Besides, PDA based on WEPSI06 detects 5 years – 1980, 1981, 1985, 2009, and 2010 – when the tail of drought (at least two sequent months with a PDA greater than zero) is observed in them, and the amount of cereal yield is lower than the previous year (i.e., the cereal yield graph is descending); it also identifies that in 2005, which is a white year, the cereal yield graph is ascending.

Generally, a growing pattern in cereal yield and crop production is observed during our study horizon. This is because cereal yield and crop productions do not depend on drought alone but are also influenced by other factors, such as agricultural land and technology. For example, El Salvador's agricultural land grew from 14,100 km^2 (or 68.05% of the land area) in

1980 to 15,350 km^2 (or 74.08% of the land area) in 2010 (Khoshnazar *et al.* 2021a, 2021b). There are some other descriptions for the rise or drop in the cereal yield graph. For example, 1992 has a tail of drought in Figure 9, while it has a local maximum in Figure 10. That is because 1992 was the end of the civil war in El Salvador, which affected the agricultural activity (e.g., increasing the number of agricultural labors) and harvesting efficiency of the country. We could not justify the local minimum in Figure 10 in 1997, based on our available information. We are only aware that this year experienced a high unemployment rate (The World Bank Group 2020). On the other hand, after consulting with experts from the area, we found out that changing in governmental policies, and utilizing more efficient agricultural equipment have led to a local maximum in 1998 (in Figure 9), with the tail of drought observed in that year in Figure 10 (Encyclopedia of the Nations 2021).

As Figure 10 shows the ascent and descent of the crop and cereal yield graphs are the same except in 1987 and 1988, when the crop graph is descending but the cereal graph is ascending. There should be another probable occurrence or policy justifying this behavior of the cereal yield graph, while these years have a tail of drought in Figure 9. Furthermore, the agricultural industry in El Salvador reported heavy losses because of rainfall and its consequences, such as flood and supersaturation within our study horizon (Freshplaza 2021). This can justify the drop in cereal yield in white years by PDA based on WEPSI06. For instance, in 1982, hurricane Paul killed 1,625 people and caused $520 million in damage in Central America, including El Salvador. Similarly, hurricane Pauline in 1997 and tropical storm Arlene in 1993 impacted our studied basin (Carroll 1998).

To sum up, PDA, based on WEPSI06, detects 85% of the cereal yield drop and 70% of the cereal yield increase. Taking the discussed abnormal conditions into account, the PDA based on WEPSI06 (Figure 9) is 81% consistent with the cereal yield graph (Figure 10).

Regarding cereal yield, the period between the first of April and the end of July is the lean period in the El Salvador cereal calendar based on Food & Agriculture Organization (FAO) of the United Nations (UN) (2021). Figure 9 demonstrates that tails of drought are observed in the lean period of cereal crops in El Salvador – during 1981, 1994, 2003, and 2007, when a reduction in cereal yield also emerges. Additionally, the growing season, which starts from June and lasts until December (FAO 2021), is also sensitive to WEPSI time-series droughts, as shown by the decrease in cereal yield. This sensitivity to drought, similar to Daryanto *et al.*'s (Daryanto *et al.* 2017) statement, is observed in 10 years in Figure 10. On the other hand, as the structure of WEPSI uses ET data, it implicitly determines soil moisture variability and, therefore, vegetation water content, directly affecting agricultural droughts (Vicente-Serrano *et al.* 2010). Indices that do not consider the role of temperature, and consequently heat, could not depict the impact of this critical environmental component on crop survival, distribution, and productivity limits (Daryanto *et al.* 2017). This is while WEPSI implicitly takes the role of temperature into account and thus could be used for agricultural targets.

These observations indicate that the results of WEPSI06 could be used for the assessment of agricultural drought.

Our results are in line with Pyarali *et al.* (2022). They evaluated the performance of their high-resolution SPEI dataset (with 6-month time step) via comparing their results with 2 years (2001 and 2008) of noticeable drought events in Central Asia. Besides, the PDA based on WEPSI06 results explained well the cereal yield at country level, while Araneda-Cabrera *et al.* (2021)'s findings show the percentages of area affected by drought based on SPEI06 and the Standardized Soil Moisture Index with 12-month time step explain the variability of most cereals, and other crops in Mozambique.

3.2. Significance of this study

Because of its inputs, WEPSI can indirectly take the climate change effect into account. WEPSI softens the performance of the SPEI because it uses ET_w instead of evaporative demand (i.e., ET_p). Accordingly, WEPSI can detect some events that are not captured by the SPI but can eliminate some others indicated by the SPEI that are derived by excessive values of ET_p.

Meteorological drought indices, such as the SPI and SPEI, describe climatic anomalies without considering their hydrologic context (Kim & Rhee 2016). Hydrological drought indices, such as the SRI, represent the impact of climate anomalies on present hydrologic conditions, as they are controlled by physical processes on the surface (Shukla & Wood 2008). Our results show a high correlation and MI between WEPSI06 and SRI06. These results indicate that WEPSI can depict a more accurate land surface status by linking meteorological and hydrological drought indices.

ET affects R (Vicente-Serrano *et al.* 2010), so the SRI can depict ET_a indirectly. Then, WEPSI, which, on the one hand, relatively reflects the SRI status and, on the other hand, uses ET, can indicate moisture conditions on the land surface. Additionally, our results showed a high similarity between the SRI with the 6-month time step (SRI06) and the Lempa

River streamflow, suggesting that SRI06 reflects the basin's most accurate condition. The results again indicate that WEPSI can be used for agricultural drought assessments.

The proposed WEPSI drought index meets all requirements suggested by Nkemdirim and Weber for a drought index (Nkemdirim & Weber 1999; Vicente-Serrano *et al.* 2010), including its use for different purposes. Drought characteristics, such as drought severity, intensity, and duration (the start and the end of the phenomenon), can also be calculated with WEPSI. Furthermore, WEPSI can be calculated worldwide and under various climates, including semi-arid regions as in this research (Global Environment Facility 2019) and can provide a spatial and temporal depiction of drought variation.

4. CONCLUSIONS

This research introduced WEPSI, which uses WS as its input. WS is calculated using P and ET_w. We embed ET_w into the structure of WEPSI to account for the water demand and P for the water supply. This paper also presents a procedure for ET_w calculation based on the asymmetric CR that links ET_p, ET_a, and ET_w.

We tested WEPSI in the Lempa River basin, which is the longest river in Central America and whose climate is semi-arid. The basin is sub-divided into eight sub-basins for its modeling with the WEAP system. ET_w is calculated with ET_p and ET_a derived from WEAP.

We compared WEPSI with two meteorological drought indices (SPI and SPEI) and a hydrological drought index (SRI) via data derived from WEAP. The performance evaluation procedure includes a r^2, RMSE, MAD, and an approach based on MI. The results show that WEPSI has the highest r and MI compared with the three other indices, indicating that WEPSI can be used for meteorological, agricultural, and hydrological drought monitoring.

Finally, drought events based on WEPSI were compared with El Niño–La Niña years, as well as with El Salvador's annual cereal yield. The results indicate that WEPSI is also helpful for agricultural drought assessments because it captures the most critical points of El Salvador's cereal yield (i.e., the local maximum and minimum points).

These research outcomes are useful for researchers and policymakers in drought calculation, monitoring, risk assessment, and forecasting. As a future research direction, the application of remote sensing data in calculating WEPSI can be investigated to facilitate the application of WEPSI in other basins. We also suggest testing WEPSI in other case studies and with other purposes. WEPSI's application for drought risk assessment is likewise foreseen.

ACKNOWLEDGEMENTS

Authors thank the grant no. 2579 of the Prince Albert II of Monaco Foundation. V.D.M. thanks the Mexican National Council for Science and Technology (CONACYT) and Alianza FiiDEM for the study grand 217776/382365.

AUTHOR CONTRIBUTION

A.K. conceptualized the study and was involved in methodology, investigation, data processing, validation, software, and wrote the original draft; G.A.C.P. conceptualized the study and was involved in project administration, supervision, and review; V.D.M. conceptualized the study and was involved in methodology, data processing, writing, review, and editing; M.A. conceptualized the study and was involved in methodology and reviewing; R.A.C.P. was involved in data processing, software, and review. All authors have read and agreed to the published version of the manuscript.

DATA AVAILABILITY STATEMENT

All data used for or generated from this study is freely available through public open-source platforms. WEAP hydrological simulations are available in Microsoft Excel format, the drought indices calculations, incl. WEPSI, are available in Microsoft Excel format. The dataset Lempa River Basin Wet-environment Evapotranspiration and Precipitation Standardized Index (WEPSI) is available from http://www.hydroshare.org/resource/b3249a7327ab4bd3a69db091430e1b9d (Khoshnazar *et al.* 2021b).

CONFLICT OF INTEREST

The authors declare there is no conflict.

REFERENCES

Abdelkader, M. & Yerdelen, C. 2021 Hydrological drought variability and its teleconnections with climate indices. *Journal of Hydrology* **605**, 127290.

Al Balasmeh, O., Babbar, R. & Karmaker, T. 2020 A hybrid drought index for drought assessment in Wadi Shueib catchment area in Jordan. *Journal of Hydroinformatics* **22** (4), 937–956.

Aminzadeh, M. & Or, D. 2014 Energy partitioning dynamics of drying terrestrial surfaces. *Journal of Hydrology* **519**, 1257–1270.

Aminzadeh, M., Roderick, M. L. & Or, D. 2016 A generalized complementary relationship between actual and potential evaporation defined by a reference surface temperature. *Water Resources Research* **52** (1), 385–406.

Araneda-Cabrera, R. J., Bermúdez, M. & Puertas, J. 2021 Assessment of the performance of drought indices for explaining crop yield variability at the national scale: methodological framework and application to Mozambique. *Agricultural Water Management* **246**, 106692.

Bouchet, R. J. 1963 Evapotranspiration réelle et potentielle, signification climatique. *IAHS Publications* **62**, 134–142.

Brito, S. S. B., Cunha, A. P. M., Cunningham, C., Alvalá, R. C., Marengo, J. A. & Carvalho, M. A. 2018 Frequency, duration and severity of drought in the Semiarid Northeast Brazil region. *International Journal of Climatology* **38** (2), 517–529.

Carroll, A. 1998 *Natural Hazards of North America*. Available from: https://catalogue.nla.gov.au/Record/7045960.

Corzo, P., Diaz, V. & Laverde, M. 2018 Spatiotemporal hydrological analysis. *International Journal of Hydrogen* **2** (1), 25–26.

Corzo Perez, G., Van Huijgevoort, M., Voß, F. & Van Lanen, H. 2011 On the spatio-temporal analysis of hydrological droughts from global hydrological models. *Hydrology and Earth System Sciences* **15** (9), 2963–2978.

Daryanto, S., Wang, L. & Jacinthe, P.-A. 2017 Global synthesis of drought effects on cereal, legume, tuber and root crops production: a review. *Agricultural Water Management* **179**, 18–33.

Dash, S. S., Sahoo, B. & Raghuwanshi, N. S. 2021 How reliable are the evapotranspiration estimates by soil and water assessment tool (SWAT) and variable infiltration capacity (VIC) models for catchment-scale drought assessment and irrigation planning? *Journal of Hydrology* **592**, 125838.

Dhungel, S. & Barber, M. E. 2018 Estimating calibration variability in evapotranspiration derived from a satellite-based energy balance model. *Remote Sensing* **10** (11), 1695.

Diaz, V., Perez, G. A. C., Van Lanen, H. A., Solomatine, D. & Varouchakis, E. A. 2020 An approach to characterise spatio-temporal drought dynamics. *Advances in Water Resources* **137**, 103512.

Diaz Mercado, V., Corzo Perez, G., Van Lanen, H. A. & Solomatine, D. 2018 Comparative analysis of two evaporation-based drought indicators for large-scale drought monitoring. In *Paper Presented at the EGU General Assembly Conference Abstracts*.

El Salvador's Ministry of Environment and Natural Resources (MARN) 2019a Available from: https://www.marn.gob.sv/.

El Salvador's Ministry of Environment and Natural Resources (MARN) 2019b *Water Resources Maps*. Available from: https://web.archive.org/web/20090422151648/http://snet.gob.sv/cd2/SeccionSIG/map_hi.htm.

Encyclopedia of the Nations. 2021 *El Salvador – Agriculture*. Available from: https://www.nationsencyclopedia.com/economies/Americas/El-Salvador-AGRICULTURE.html.

Fanok, L., Beltrán, B. J., Burnham, M. & Wardropper, C. B. 2022 Use of water decision-support tools for drought management. *Journal of Hydrology* 127531.

Fisher, J. B., Whittaker, R. J. & Malhi, Y. 2011 ET come home: potential evapotranspiration in geographical ecology. *Global Ecology and Biogeography* **20** (1), 1–18.

Food and Agriculture Organization (FAO) of the United Nations (UN). 2021 *GIEWS – Global Information and Early Warning System. Country Briefs. El Salvador*. Available from: http://www.fao.org/giews/countrybrief/country.jsp?code=SLV&lang=en.

Freshplaza. 2021 *Agricultural Industry in El Salvador Reports Heavy Losses due to Rainfall*. Available from: https://www.freshplaza.com/article/9267702/agricultural-industry-in-el-salvador-reports-heavy-losses-due-to-rainfall/.

Global Environment Facility. 2019 *Fostering Water Security in the Trifinio Region: Promoting the Formulation of A TDA/SAP for its Transboundary Lempa River Basin*. Available from: https://www.thegef.org/project/fostering-water-security-trifinio-region-promoting-formulation-tdasap-its-transboundary.

Granger, R. 1989 A complementary relationship approach for evaporation from nonsaturated surfaces. *Journal of Hydrology* **111** (1–4), 31–38.

Han, S. & Tian, F. 2020 A review of the complementary principle of evaporation: from the original linear relationship to generalized nonlinear functions. *Hydrology and Earth System Sciences* **24** (5), 2269–2285.

Helman, P. & Tomlinson, R. 2018 Two centuries of climate change and climate variability, East Coast Australia. *Journal of Marine Science Engineering* **6** (1), 3.

Hernández, W. 2005 Nacimiento y Desarrollo del río Lempa. *MARN/SNET*.

Hobeichi, S., Abramowitz, G. & Evans, J. P. 2021 Robust historical evapotranspiration trends across climate regimes. *Hydrology and Earth System Sciences* **25** (7), 3855–3874.

Homdee, T., Pongput, K. & Kanae, S. 2016 A comparative performance analysis of three standardized climatic drought indices in the Chi River basin, Thailand. *Agriculture and Natural Resources* **50** (3), 211–219.

Jennewein, J. S. & Jones, K. W. 2016 Examining 'willingness to participate'in community-based water resource management in a transboundary conservation area in Central America. *Water Policy* **18** (6), 1334–1352.

Kahler, D. M. & Brutsaert, W. 2006 Complementary relationship between daily evaporation in the environment and pan evaporation. *Water Resources Research* **42** (5), W05413.

Karim, M. R. & Rahman, M. A. 2015 Drought risk management for increased cereal production in Asian least developed countries. *Weather and Climate Extremes* **7**, 24–35.

Khoshnazar, A., Corzo Perez, G. A. & Diaz, V. 2021a Spatiotemporal drought risk assessment considering resilience and heterogeneous vulnerability factors: Lempa Transboundary River Basin in the Central American dry corridor. *Journal of Marine Science and Engineering* **9** (4), 386.

Khoshnazar, A., Corzo Perez, G. A., Diaz, V. & Aminzadeh, M. 2021b Lempa river basin wet-environment evapotranspiration and precipitation standardized index (WEPSI) data. *HydroShare*. Available from: http://www.hydroshare.org/resource/b3249a7327ab4bd3a69db091430e1b9d.

Kim, D. & Rhee, J. 2016 A drought index based on actual evapotranspiration from the Bouchet hypothesis. *Geophysical Research Letters* **43** (19), 10,277–210,285.

Kim, J.-S., Jain, S., Lee, J.-H., Chen, H. & Park, S.-Y. 2019 Quantitative vulnerability assessment of water quality to extreme drought in a changing climate. *Ecological Indicators* **103**, 688–697.

Koppa, A., Alam, S., Miralles, D. G. & Gebremichael, M. 2021 Budyko-based long-term water and energy balance closure in global watersheds from earth observations. *Water Resources Research* **57** (5), e2020WR028658.

Kumar, P., Masago, Y., Mishra, B. K. & Fukushi, K. 2018 Evaluating future stress due to combined effect of climate change and rapid urbanization for Pasig-Marikina River, Manila. *Groundwater for Sustainable Development* **6**, 227–234.

Lewis, J., Rowland, J. & Nadeau, A. 1998 Estimating maize production in Kenya using NDVI: some statistical considerations. *International Journal of Remote Sensing* **19** (13), 2609–2617.

Lu, Z., Zhao, Y., Wei, Y., Feng, Q. & Xie, J. 2019 Differences among evapotranspiration products affect water resources and ecosystem management in an Australian catchment. *Remote Sensing* **11** (8), 958.

Mahmoodzadeh, A., Nejati, H. R., Mohammadi, M., Ibrahim, H. H., Rashidi, S. & Rashid, T. A. 2022 Forecasting tunnel boring machine penetration rate using LSTM deep neural network optimized by grey wolf optimization algorithm. *Expert Systems with Applications* 118303.

McKee, T. B., Doesken, N. J. & Kleist, J. 1993 The relationship of drought frequency and duration to time scales. In *Paper Presented at the Proceedings of the 8th Conference on Applied Climatology*.

Mera, Y. E. Z., Vera, J. F. R. & Pérez-Martín, M. Á. 2018 Linking El Niño Southern Oscillation for early drought detection in tropical climates: the Ecuadorian coast. *Science of The Total Environment* **643**, 193–207.

Mukherjee, S., Mishra, A. & Trenberth, K. E. 2018 Climate change and drought: a perspective on drought indices. *Current Climate Change Reports* **4** (2), 145–163.

National Oceanic and Atmospheric Administration 2015 *The El Niño Southern Oscillation (ENSO) is one of the Most Important Climatic Phenomena on Earth*. Available from: https://www.noaa.gov/education/resource-collections/weather-atmosphere/el-nino.

Nkemdirim, L. & Weber, L. 1999 Comparison between the droughts of the 1930s and the 1980s in the southern prairies of Canada. *Journal of Climate* **12** (8), 2434–2450.

Oti, J. O., Kabo-Bah, A. T. & Ofosu, E. 2020 Hydrologic response to climate change in the Densu River Basin in Ghana. *Heliyon* **6** (8), e04722.

Palmer, W. C. 1965 *Meteorological Drought (Vol. 30)*. US Department of Commerce, Weather Bureau, Washington DC.

Palmer, W. C. 1968 *Keeping Track of Crop Moisture Conditions, Nationwide: the new Crop Moisture Index*.

Pant, S. & Kumar, S. 2022 IFS and SODA based computational method for fuzzy time series forecasting. *Expert Systems with Applications* **209**, 118213.

Peters, E., Torfs, P., Van Lanen, H. A. & Bier, G. 2003 Propagation of drought through groundwater – a new approach using linear reservoir theory. *Hydrological Processes* **17** (15), 3023–3040.

Priestley, C. H. B. & Taylor, R. J. 1972 On the assessment of surface heat flux and evaporation using large-scale parameters. *Monthly Weather Review* **100** (2), 81–92.

Pyarali, K., Peng, J., Disse, M. & Tuo, Y. 2022 Development and application of high resolution SPEI drought dataset for Central Asia. *Scientific Data* **9** (1), 1–14.

Qaisrani, Z. N., Nuthammachot, N., Techato, K., Jatoi, G. H., Mahmood, B. & Ahmed, R. 2022 Drought variability assessment using standardized precipitation index, reconnaissance drought index and precipitation deciles across Balochistan, Pakistan. *Brazilian Journal of Biology* **84**, e261001.

Seiber, J. & Purkey, D. 2015 *WEAP – Water Evaluation and Planning System User Guide for WEAP 2015*. Stockholm Environment Institute.

Sheffield, J., Goteti, G. & Wood, E. F. 2006 Development of a 50-year high-resolution global dataset of meteorological forcings for land surface modeling. *Journal of Climate* **19** (13), 3088–3111.

Shukla, S. & Wood, A. W. 2008 Use of a standardized runoff index for characterizing hydrologic drought. *Geophysical Research Letters* **35** (2), L02405.

Slater, L. J., Anderson, B., Buechel, M., Dadson, S., Han, S., Harrigan, S. & Matthews, T. 2021 Nonstationary weather and water extremes: a review of methods for their detection, attribution, and management. *Hydrology and Earth System Sciences* **25** (7), 3897–3935.

Sorí, R., Vázquez, M., Stojanovic, M., Nieto, R., Liberato, M. L., Gimeno, L. J. N. H. & Sciences, E. S. 2020 Hydrometeorological droughts in the Miño–Limia–Sil hydrographic demarcation (northwestern Iberian peninsula): the role of atmospheric drivers. *Natural Hazards and Earth System Sciences* **20** (6), 1805–1832.

Speich, M. J. 2019 Quantifying and modeling water availability in temperate forests: a review of drought and aridity indices. *iForest-Biogeosciences and Forestry* **12** (1), 1.

Sutanto, S. J. & Van Lanen, H. A. 2021 Streamflow drought: implication of drought definitions and its application for drought forecasting. *Hydrology and Earth System Sciences* **25** (7), 3991–4023.

Tabari, H., Paz, S. M., Buekenhout, D. & Willems, P. 2021 Comparison of statistical downscaling methods for climate change impact analysis on precipitation-driven drought. *Hydrology and Earth System Sciences* **25** (6), 3493–3517.

The World Bank Group 2020 *Unemployment, Total (% of Total Labor Force) (Modeled ILO Estimate) - El Salvador*. Available from: https://data.worldbank.org/indicator/SL.UEM.TOTL.ZS?end=2020&locations=SV&start=1991.

The World Bank Group 2021 *Cereal Yield (kg per Hectare) - El Salvador*. Available from: https://data.worldbank.org/indicator/AG.YLD.CREL.KG?end=2018&locations=SV&start=1961.

The World Bank Group 2022 *Metadata Glossary – Crop Production Index (2014–2016=100)*. Available from: https://databank.worldbank.org/metadataglossary/world-development-indicators/series/AG.PRD.CROP.XD.

Vergara, J. R. & Estévez, P. A. 2014 A review of feature selection methods based on mutual information. *Neural Computing and Applications* **24** (1), 175–186.

Vicente-Serrano, S. M. 2006 Differences in spatial patterns of drought on different time scales: an analysis of the Iberian Peninsula. *Water Resources Management* **20** (1), 37–60.

Vicente-Serrano, S. M., Beguería, S. & López-Moreno, J. I. 2010 A multiscalar drought index sensitive to global warming: the standardized precipitation evapotranspiration index. *Journal of Climate* **23** (7), 1696–1718.

Vicente-Serrano, S. M., Miralles, D. G., Domínguez-Castro, F., Azorin-Molina, C., El Kenawy, A., McVicar, T. R. & Peña-Gallardo, M. 2018 Global assessment of the Standardized Evapotranspiration Deficit Index (SEDI) for drought analysis and monitoring. *Journal of Climate* **31** (14), 5371–5393.

Wang, D., Hejazi, M., Cai, X. & Valocchi, A. J. 2011 Climate change impact on meteorological, agricultural, and hydrological drought in central Illinois. *Water Resources Research* **47** (9), W09527.

Wang, Y., Yang, J., Chen, Y., Su, Z., Li, B., Guo, H. & De Maeyer, P. 2020 Monitoring and predicting drought based on multiple indicators in an Arid Area, China. *Remote Sensing* **12** (14), 2298.

Warter, M. M., Singer, M. B., Cuthbert, M. O., Roberts, D., Caylor, K. K., Sabathier, R. & Stella, J. 2021 Drought onset and propagation into soil moisture and grassland vegetation responses during the 2012–2019 major drought in Southern California. *Hydrology and Earth System Sciences* **25** (6), 3713–3729.

Wells, N., Goddard, S. & Hayes, M. J. 2004 A self-calibrating Palmer drought severity index. *Journal of Climate* **17** (12), 2335–2351.

Wen, W., Timmermans, J., Chen, Q. & van Bodegom, P. M. 2021 A review of remote sensing challenges for food security with respect to salinity and drought threats. *Remote Sensing* **13** (1), 6.

Wilhite, D. A. & Glantz, M. H. 1985 Understanding: the drought phenomenon: the role of definitions. *Water International* **10** (3), 111–120.

Xiao, M., Yu, Z., Kong, D., Gu, X., Mammarella, I., Montagnani, L. & Lohila, A. 2020 Stomatal response to decreased relative humidity constrains the acceleration of terrestrial evapotranspiration. *Environmental Research Letters* **15** (9), 094066.

Yihdego, Y., Vaheddoost, B. & Al-Weshah, R. A. 2019 Drought indices and indicators revisited. *Arabian Journal of Geosciences* **12** (3), 69.

Zargar, A., Sadiq, R., Naser, B. & Khan, F. I. 2011 A review of drought indices. *Environmental Reviews* **19** (NA), 333–349.

Zhang, J., Bai, Y., Yan, H., Guo, H., Yang, S. & Wang, J. 2020 Linking observation, modelling and satellite-based estimation of global land evapotranspiration. *Big Earth Data* **4** (2), 94–127.

Zheng, C., Jia, L., Hu, G. & Lu, J. 2019 Earth observations-based evapotranspiration in Northeastern Thailand. *Remote Sensing* **11** (2), 138.

First received 31 May 2022; accepted in revised form 17 October 2022. Available online 27 October 2022